Prediction of barrel swirl and turbulence in recriprocating engines using a phenomenological model

Benjamin, S.F.

C465/013/93

Prediction of barrel swirl and turbulence in reciprocating engines using a phenomenological model

S F BENJAMIN, BSc, PhD, ARCS
School of Engineering, Coventry University

SYNOPSIS A phenomenological model has been developed to describe the behaviour of barrel (or tumble) swirl and turbulence during the compression stroke of a reciprocating engine. Parametric studies are described which illustrate the effect of engine geometry and flow conditions on the development of swirl and turbulence in the chamber.

NOTATION

B	cylinder bore
C_D, $C_{\varepsilon 1}$, $C_{\varepsilon 2}$	constants in turbulence model
C_f	friction coefficient
ds	elemental length at cylinder wall
dS	elemental surface area
dV	elemental volume
k	turbulent kinetic energy
l	conrod length
l_s	turbulent length scale
L	chamber height
M	mass of cylinder contents
r	crank throw
R	cylinder radius
R_e	Reynolds number
S	swirl ratio
T	torque
u	fluid velocity
u'	turbulence rms
u^*	friction velocity
U	maximum swirl velocity at periphery of vortex
V_p	mean piston speed
V_s	instantaneous piston speed
V_{wall}	fluid velocity near the wall
W	width of elemental vortex
x_i, x, y, z	co-ordinate axes
y^+	non-dimensional distance from wall
α	circumferential angle around bore
ε	energy dissipation rate
θ	crank angle
υ	kinematic viscosity
υ_t	turbulent kinematic viscosity
ρ	fluid density
τ	shear stress
ω	initial swirl level
ω_e	engine speed
Ω	angular momentum of cylinder contents

1 INTRODUCTION

The production of swirl and turbulence in spark ignition engines has long been recognised as essential if good combustion, improved fuel economy and reduced emissions are to be realised.

The traditional approach has been to generate 'axial' swirl; that is swirl around a vertical axis of rotation. This is readily achieved using a single inlet port directed in such a way to produce a high tangential component of flow into the chamber. The difficulty with this concept has been how to harness the swirl energy to efficiently enhance flame propagation across the chamber. Swirling flow on its own will essentially only serve to advect the flame around the chamber rather than promote mixing and may, indeed, blow the flame out. It has also been shown that axial swirl can reduce in-cylinder turbulence (1). Hence mechanisms need to found for breaking the bulk swirl down into turbulence energy; this being a much more efficient source for promoting flame growth.

An alternative approach has become popular in recent years in which the swirl is generated around a horizontal axis. This is variously referred to as barrel or tumble swirl. Barrel swirl can be readily generated in four-valve chambers as shown in figure 1. With two inlet ports, suitably designed, the flow can be directed over the top of the valves and enters the chamber producing the aforementioned swirling motion. The perceived advantage of this approach is that during compression, the distorted vortex naturally provides the high shear stresses needed to generate the turbulence whilst at the same time reducing the energy of the main vortex. Another advantage of barrel swirl over axial swirl is that in four-valve chambers the same swirl level can be achieved as with a two-valve

chamber albeit with a greater induced flow and hence more power (2).

Experimental and some theoretical work has recently been undertaken to study the behaviour of barrel swirl flows and their effect on engine performance (2)-(10). A complete description of the flow field is difficult to obtain experimentally due to the inherent difficulties of obtaining comprehensive in-cylinder flow measurements throughout the chamber. Computational fluid dynamics (CFD), offers the possibility of providing such information and examples of this approach (specifically for barrel swirl type flows) can be found in the work of Gosman et al (3) and Le Coz et al (4). In particular, CFD offers the prospect of addressing the fundamental question; what is the optimum swirl level for a given engine geometry? However the resources necessary to model these systems are considerable and the technical difficulties of modelling complex head designs with moving valves and pistons are considerable.

An alternative approach is to explore the possibility of developing a phenomenological model. This approach has been adopted for the axial swirl type chambers as described, for example, by Borgnakke et al. (11). A simple analytical phenomenological model for barrel swirl chambers has also been developed by the author (10). These models hold the prospect of providing considerable insight into the controlling parameters of these systems but at a considerable reduction in complexity (and cost) to the CFD approach. They do, of course, have their limitations but as a complementary tool in the 'armoury of techniques' available to the design engineer they can be extremely useful design aids.

This paper extends the work previously described by the author(10). In that paper a simple phenomenological model was described which predicted the behaviour of the barrel swirl vortex during the compression stroke. The model assumed a constant turbulent kinematic viscosity, υ_t (i.e. the simplest turbulence model) and demonstrated how the vortex could spin-up during compression to be degraded near the top of the stroke where high shear stresses developed. The model was shown to provide qualitative agreement with the limited experimental and theoretical data available. Model results showed however that the breakdown of the vortex depended strongly on the value of υ_t and that it was clearly necessary to incorporate a more sophisticated turbulence model .

The purpose of this paper is to extend the previous model by incorporating a two parameter $(k-\varepsilon)$ turbulence model both to predict the turbulence field and the main vortex behaviour more accurately. Parametric studies are performed on the model to show how various engine geometries and swirl fields affect the vortex behaviour during compression.

2 MODEL DEVELOPMENT

2.1 Mean flow field

For this investigation, as previously (10), the simplest engine geometry will be considered i.e. a disc or pancake chamber as shown in figure 2. The model requires a prescription of the form of the velocity field and following (10) it will be assumed that the barrel vortex spins in two-dimensional planes taking the form;

$$u_x = 2U\left(1-\frac{z^2}{R^2}\right)\frac{y}{L}$$

$$u_y = -2U\left(1-\frac{z^2}{R^2}\right)\frac{x}{W}$$

$$u_z = 0$$

Figure 3 illustrates this flow field. The vortex is assumed to be bounded by the cylinder walls and by the piston and head faces. Hence at the vortex surface $u_x = 0$ near the cylinder walls and $u_y = 0$ near the piston and head faces. This flow field, although of simple form, is expected to contain many of the features of the barrel swirl vortex and, as discussed in (10), is believed to form a reasonable basis for model development.

The development of the mean flow field can be described by applying Newton's second law to the vortex flow:

$$\frac{d\Omega}{dt} = -T \qquad (1)$$

where

Ω = angular momentum of the vortex

T = external couples

The external couples are those due to the shear forces acting at the vortex surface. The shear forces can be evaluated directly from the velocity field gradients at the vortex periphery but this requires a detailed prescription of the flow field and boundary layers at the chamber walls. The approach adopted here, as described in (10), is to treat the shear forces in two parts. Firstly, if we ignore the wall boundary layers (essentially assuming a slip condition at the walls) then the internal fluid shear stresses τ_s will exert a self-induced restraining couple at the vortex surface through internal mixing. Secondly, the effect of the boundary layer is accounted for through wall friction stresses τ_w which act as a further restraining couple.

To evaluate the external couples requires integrating the surface shear stress moments over the vortex surface. Following (10) we can consider first an elemental vortex as shown in figure 4. This vortex is situated at plane z and is of height L and width W. The external torque, T, is given by:

$$T = \int_{surf} (\tau_s + \tau_w) WL \, ds + \int_{surf} (\tau_s + \tau_w) WL \, dz$$

The integrals on the right hand side represent the contributions from the cylinder walls and piston/head faces respectively. The evaluation of these integrals is described in the appendix and yields:

$$T = \frac{3UM\upsilon_t}{2}\left(\frac{1}{L} + \frac{16}{9\pi B}\right) + 0.72 C_f M U^2 \qquad (2)$$

where the first and second terms on the right hand side are the torques resulting from the internal shear stresses and the wall boundary layers respectively.

The angular momentum can be obtained as below:

$$\Omega = \int_{vol} (u_x y - u_y x) \rho \, dx \, dy \, dz$$

and after evaluation (see appendix) gives:

$$\Omega = \frac{MU}{8}(L + 1.81R) \qquad (3)$$

Hence finally after substituting equations (2) and (3) into equation (1), we obtain:

$$\frac{d}{dt}\left\{\frac{MU}{8}(L + 1.81R)\right\} = \frac{-3UM\upsilon_t}{2}\left(\frac{1}{L} + \frac{16}{9\pi B}\right) - 0.72 C_f M U^2 \qquad (4)$$

2.2 The turbulence model

The turbulence model employed is the $k-\varepsilon$ model as described by Launder and Spalding (12) and developed by Borgnakke et al (11). Here k represents the turbulent kinetic energy and ε its dissipation rate. From k and ε a turbulent length scale l_s and turbulent kinematic viscosity υ_t can be derived as given below:

$$l_s = \frac{C_D k^{3/2}}{\varepsilon} \qquad \text{and} \qquad \upsilon_t = l_s k^{1/2}$$

The model expresses the rate of change of k and ε as follows:

Rate of change = Rate of production + Rate of dissipation + Diffusion flux

The rate of production can be expressed as the sum of that due to compression plus that due to the shear field. This can be expressed as (see Borgnakke et al (11)):

Rate of production (k)

$$= \frac{2}{3} k \frac{\partial \rho}{\partial t} + \tau_{ij} \frac{\partial u_i}{\partial x_j}$$

Rate of production (ε)

$$= \frac{4}{3} \varepsilon \frac{\partial \rho}{\partial t} + C_{\varepsilon 1} \frac{\varepsilon}{k} \tau_{ij} \frac{\partial u_i}{\partial x_j} \qquad i \neq j$$

where τ_{ij}, the stress tensor is given by:

$$\tau_{ij} = \rho \upsilon_t \left(\frac{\partial u_i}{\partial x_j} + \frac{\partial u_j}{\partial x_i}\right)$$

The dissipation term for the k-equation is simply $\rho\varepsilon$ whilst in the ε-equation it can be expressed as $\rho C_{\varepsilon 1}\left(\varepsilon^2/k\right)$ (see Borgnakke et al (11)).

The rate equations can now be integrated over the combustion chamber volume and the diffusion flux then becomes a flux across the vortex surface as follows:

$$\int_{vol} \rho \frac{dk}{dt} \, dV = \int_{vol} \left(\frac{2}{3} k \frac{d\rho}{dt} + \tau_{ij} \frac{\partial u_i}{\partial x_j} - \rho\varepsilon\right) dV + \int_{surf} \text{Flux}_k \, dS$$

$$\int_{vol}\rho\frac{d\varepsilon}{dt}\,dV=\int_{vol}\left(\frac{4}{3}\varepsilon\frac{d\rho}{dt}+C_{\varepsilon1}\frac{\varepsilon}{k}\tau_{ij}\frac{\partial u_i}{\partial x_j}-\rho C_{\varepsilon2}\frac{\varepsilon^2}{k}\right)dV+$$

$$\int_{surf}\text{Flux}_\varepsilon\,dS$$

These integrals can be evaluated (see appendix) to give:

$$\frac{dk}{d\theta}=-\frac{2}{3L}\frac{dL}{d\theta}k+\frac{5\upsilon_t}{2\omega_e}\left(\frac{1}{L^2}+\frac{28}{15B^2}-\frac{512}{75BL}\right)-\frac{\varepsilon}{\omega_e}-$$

$$\frac{2}{\omega_e}\left\{\frac{\upsilon_{1eq}(k-k_{1eq})}{0.5By_{1eq}}+\frac{\upsilon_{2eq}(k-k_{2eq})}{Ly_{2eq}}\right\}\qquad(5)$$

$$\frac{d\varepsilon}{d\theta}=-\frac{4}{3L}\frac{dL}{d\theta}\varepsilon+\frac{5\upsilon_t}{2\omega_e}\left(\frac{1}{L^2}+\frac{28}{15B^2}-\frac{512}{75BL}\right)\frac{C_{\varepsilon1}\varepsilon}{k}-\frac{C_{\varepsilon2}\varepsilon^2}{\omega_e k}-$$

$$\frac{2}{\omega_e}\left\{\frac{\upsilon_{1eq}(\varepsilon-\varepsilon_{1eq})}{0.5By_{1eq}}+\frac{\upsilon_{2eq}(\varepsilon-\varepsilon_{2eq})}{Ly_{2eq}}\right\}\qquad(6)$$

Equations (4), (5) and (6) are three non-linear coupled ordinary differential equations for U, k and ε. These were solved with a Runge-Kutta routine using the NAG software library.

3 MODEL RESULTS

3.1 Reference test case

This section investigates the effect of various engine geometries and flow field parameters on the behaviour of the barrel swirl vortex and turbulence field during compression. For this study the reference conditions shown in table 1 have been taken.

Table 1 Reference conditions

Engine geometry	
bore	.08m
stroke	.08m
compression ratio	10:1
conrod length	.14m
engine speed	2000 rpm
IVC	BDC
Flow field at IVC	
swirl ratio	2.0
turbulence intensity	1.0
turbulence length scale	0.00222m

Figure 5 shows predictions for these reference conditions. Swirl is seen to reach a maximum at 305° after which it then decays rapidly to TDC. Turbulence intensity, after an initial reduction, increases rapidly after 300°. By TDC it has increased by 70%. This demonstrates how the energy in the main barrel swirl vortex is transformed into turbulence-the major feature of this type of flow field.

The exact mechanism of this transformation is a result of the complex interactions of the main flow and turbulence fields. Equations (5)-(6) show that the rate of change of k and ε is determined by four elements; namely production by compression and shear , dissipation and a wall sink. These are shown in figure 6.

Figure 6 shows that initially dissipation is greater than the combined production terms and hence u' is reduced until about 270°. Production due to compression and shear increases rapidly from 300° dominating dissipation and hence k increases. Towards the end of the stroke production declines. The contribution from the wall flux is small with greatest losses occurring later in the stroke where higher surface-to-volume ratios are found.

It is perhaps useful to examine the individual terms in equation (5) so as to gain an understanding of their contributions to the turbulence profiles.

Production by compression is proportional to the product of k and $-V_s/L$ where V_s is the instantaneous piston speed (see equations (5)). Figure 7 shows $-V_s/L$ throughout the compression process. At the stroke extremities $-V_s/L$ is zero and peaks at 330°. The form of the production by compression term reflects this parameter however peak production occurs later than 330° because the maximum value of k occurs later in the stroke.

Production by shear is strongly related to υ_t and the rate of strain viz. $\upsilon_t\left(\partial u_i/\partial x_j+\partial u_j/\partial x_i\right)\partial u_i/\partial x_j$. The strain field, well into compression behaves $\sim U/L$. For this engine geometry, with *no* restraining couples, U will approximately double from BDC to TDC (**10**) (the spin-up effect, due to conservation of angular momentum) and as L is reduced the rate of strain would increase considerably. However shear stresses do exist and their associated restraining couples (which are proportional to the rate of strain) will also increase thus tending to reduce swirl. The net effect of these two processes determines the swirl velocities during the compression stroke. Figure 8 shows the components contributing to turbulence production by shear. Turbulent viscosity is the product of length scale and $k^{1/2}$, and the variation of υ_t, l_s and k are shown in figure 8. In the first half of the stroke strain is relatively small as is υ_t . As L reduces, the rate of strain increases because

the opposing effects of spin-up and vortex degradation result in U remaining relatively constant. Also υ_t increases with production of k and this further enhances shear production. This continues up to 345° where the main vortex is degrading considerably (see figure 5) due to the large rate of strain and hence shear . It can be seen that although υ_t and rate of strain are relatively high at 345° it is the strain field which contributes most to the rate of production by shear at this point. As the vortex collapses so does the rate of strain and hence production due to the shear/strain interaction.

The above shows how production by compression and shear serve to increase the production of turbulent kinetic energy up to 355° after which dissipation dominates. A particular feature of this flow field is the dominant effect of production by shear over compression . This has also been demonstrated by Gosman et al (3) using CFD for a similar type of flow field.

This analysis also shows that the development of the flow field depends on complex interactions between various physical mechanisms and is expected to depend on engine geometry as well as the initial state of the flow field. The following sections illustrate the effect of varying some of the model parameters both to assess the sensitivity of predictions and to provide an indication of possible ways of controlling the flow field for efficient combustion.

3.2 Effect of swirl ratio

Figure 9 illustrates the effect of varying the swirl ratio, S. For these simulations it has been assumed that initial length scales are the same but that u' at IVC is proportional to swirl ratio. With low swirl the spin-up of the vortex is stronger and a relatively high level of swirl persists even at TDC. The increase in turbulence intensity is also greatest but the absolute level of u' is, however, substantially lower than for the higher swirl ratio simulations.

Figure 10 shows the rate of production and dissipation for two swirl levels. The magnitudes for the higher swirl level are considerably higher due to the higher initial level of turbulence which also increases the levels of υ_t as shown in figure 11. This increases the arresting torque as well as shear production of k . The higher torque reduces the spin-up of the vortex considerably. Whereas for the lowest swirl level the spin-up effect is able to increase the relative swirl velocities by 35% the swirl velocities are almost continuously reducing for the highest swirl ratio case. This effect was demonstrated in (10) which showed analytically the high sensitivity of swirl development to υ_t. Increasing swirl ratio also increases the rate of strain $(\propto S)$ and hence the rate of production by shear of turbulent kinetic energy $\left(\propto \upsilon_t S^2\right)$.

Although production of k by compression and shear is much higher for the larger swirl ratio, dissipation is also high. The net effect is that at TDC the values of u' have only been increased by a factor of 1.3 for the highest swirl level, whereas for the lowest swirl case they have increased by a factor of 2. However there is a higher level of residual swirl for the low swirl case and this could be an undesirable feature as discussed earlier.

3.3 Effect of compression ratio

Figure 12 shows the effect of compression ratio. Increasing the compression ratio from 7:1 to 13:1 only significantly affects the latter part of the stroke as might be expected. Swirl arrestment is accelerated and turbulence intensity increased from about 310° onwards. Figure 13 shows that increasing compression ratio from 7:1 to 13:1 increases the rate of production by compression by a factor of 3.7. Production by shear is also increased because chamber height is reduced i.e. rate of strain is higher.

3.4 Effect of bore size

Figure 14 shows that by increasing the bore size the swirl velocity is increased throughout the stroke. Turbulent intensity is at first reduced and then is increased over the smaller bore engines. In the initial part of the stroke the strain field behaves as $\sim (U/L+U/B)$. Hence for the larger bore engine the rate of strain is reduced as is turbulent production by shear and hence u' and shear stresses. Consequently the swirl is higher. Later in the stroke the rate of strain behaves as $\sim U/L$ because $L<<B$. The higher velocities for the larger bore engine thus increase the rate of strain and consequently turbulent production by shear $\sim (U/L)^2$.

3.5 Effect of stroke

Figure 15 shows the effect of varying the engine stroke. As the stroke changes so does the mean piston speed, V_p and it has been assumed that u'/V_p at IVC is the same for each case i.e. the rms. and swirl velocity scales with mean piston speed at IVC. The initial length scale has been assumed to remain the same for each case. The longer stroke therefore implies that initially higher values of u' and hence υ_t will be observed. The results indicate that higher normalised swirl and smaller values of turbulence intensities are observed with the longer stroke engine. With no arresting torque a longer stroke would imply a greater spin-up effect. However a larger value of ν_t increases the arresting torque. The net effect for this geometry produces

higher levels of swirl velocity. Although turbulent intensity is lower for the longest stroke u' is actually higher because of the higher mean piston speed i.e. production of k later in the stroke is higher for the longer stroke engine.

3.6 Effect of initial level of turbulent intensity

This and the subsequent section examine the effect of initial conditions at IVC on the development of the barrel swirl vortex and its associated turbulence field. This is considered important as it illustrates the sensitivity of predictions to initial conditions and hence the accuracy with which these need to be known. Clearly it would be desirable if the whole induction process could be modelled as then only conditions at the valve need be prescribed. This, however, would be a considerable task.

Figure 16 shows the effect of varying u'/V_p by a factor of two from the reference case. Increasing u' increases υ_t and the shear stresses thus increasing swirl arrestment. This is similar to the swirl ratio effect discussed earlier. In contrast to figure 9 however the lower initial turbulence intensity actually gives the highest intensity at TDC. Late in the stroke the higher rates of strain (with $u'/V_p = 0.5$) produce greater production by shear of k. Interestingly, although initially u' varied by a factor of four the differences at TDC are only about 23% although swirl velocity varies considerably at about 330°. In summary , higher initial values of u' reduce the 'spin-up' effect and thus suppress turbulence production by shear later in the cycle.

3.7 Effect of varying length scale

Figure 17 shows the effect of varying initial length scales, l_s by a factor of four. Increasing l_s increases υ_t and hence shear stresses, turbulence production by shear and swirl arrestment. Later in the stroke this reduces the rate of strain and hence turbulence production by shear. Again a factor of four variation in initial length scales only changes the turbulence intensity by about 24% at TDC although the swirl velocity varies significantly at about 330°.

4 CONCLUSIONS

The results of these simulations illustrate that there is a complex interaction between the flow field and engine geometry. The model does illustrate quite well how the swirl energy is converted to turbulence energy mainly through production by shear and how this process can be modified (and thus controlled) through geometric changes and swirl conditions.

The main conclusions from this study may be summarised as follows:

1. A phenomenological model has been developed to describe the behaviour of barrel (or tumble) swirl and turbulence during compression for a disc-type chamber.

2. The model illustrates how turbulence energy is obtained from the swirling vortex by production from shear. This mechanism is expected to dominate that due to production by compression for most of the typical configurations encountered.

3. The level of induced swirl and the turbulence field at IVC have a significant effect on the subsequent behaviour of the vortex and turbulence fields.

4. Higher induced swirl levels cause rapid decay of the vortex and higher levels of turbulence intensity at TDC although turbulence *enhancement* is reduced.

5. Increasing the compression ratio reduces swirl velocities and increases turbulence intensities.

6. Reducing the bore size can reduce swirl velocities and turbulence energy towards the end of compression.

7. Increasing the engine stroke can result in higher normalised swirl velocities and lower turbulence intensities.

The model is clearly a simplification of the flow behaviour but is believed to provide a useful framework for examining the influence of the major parameters influencing barrel swirl flows. The question as to what are the 'optimum' flow conditions required for good combustion is a separate issue which still needs to be addressed.

Finally a comprehensive set of in-cylinder flow measurements is needed against which model predictions can be compared and refinements introduced.

REFERENCES

(1) ARCOUMANIS, C., BICEN, A. F. and WHITELAW, J. H. Effect of inlet parameters on the flow characteristics in a four-stroke model engine. SAE paper 820750, 1982

(2) BENJAMIN, S.F. The development of the GTL 'barrel swirl' combustion system with application to four-valve spark ignition engines. IMechE conference on *Combustion-engines-technology and applications*, 1988, paper C323/049, p. 203 (Mechanical Engineering Publications, London).

(3) GOSMAN, A. D., TSUI, Y. Y. and VAFIDIS, C. Flow in a model engine with a shrouded valve-a combined experimental and computational study. SAE paper 850498, 1985.

(4) LE COZ, J., HENRIOT, S. and PINCHON, P. An experimental and computational analysis of the flow field in a four-valve spark ignition engine-focus on cycle-resolved turbulence, SAE paper 900056, 1990.

(5) ARCOUMANIS, C., HU, Z., VAFIDIS, C. and WHITELAW, J. H. Tumbling motion: A mechanism for turbulence enhancement in spark-ignition engines, SAE paper 900060, 1990.

(6) HADDED, O. and DENBRATT, I. Turbulence characteristics of tumbling air motion in four-valve S.I. engines and their correlation with combustion parameters, SAE paper 910478, 1991.

(7) KHALIGHI, B. Intake-generated swirl and tumble motions in a 4-valve engine with various intake configurations-flow visualisation and particle tracking velocimetry, SAE paper 900059, 1990.

(8) OMORI, S., IWACHIDO, K., MOTOMOCHI, M., and HIRAKO, O. Effect of intake port flow on the in-cylinder tumbling air flow in multi-valve SI engines, SAE paper 910477, 1991.

(9) KENT, J. C., MIKULEC, A., RIMAL, L., ADAMCZYK, A. A., MUELLER, S. R., STEIN, R. A. and WARREN, C. C. Observations on the effects of intake-generated swirl and tumble on combustion duration, SAE paper 892096, 1989.

(10) BENJAMIN, S. F. A phenomenological model for 'barrel' swirl in reciprocating engines, *Proc. Instn Mech. Engrs.*, Part D, 1992, **206**, 63-71

(11) BORGNAKKE, C., DAVIES, G. C. and TABACZYNSKI, R. J. Predictions of in-cylinder swirl and turbulence intensity for an open chamber cup in piston engine. *Trans. SAE*, 1981, **90**, (paper 810224).

(12) LAUNDER, B. E. and SPALDING D. B. *Lectures in mathematical models of turbulence*, 1972, (Academic Press).

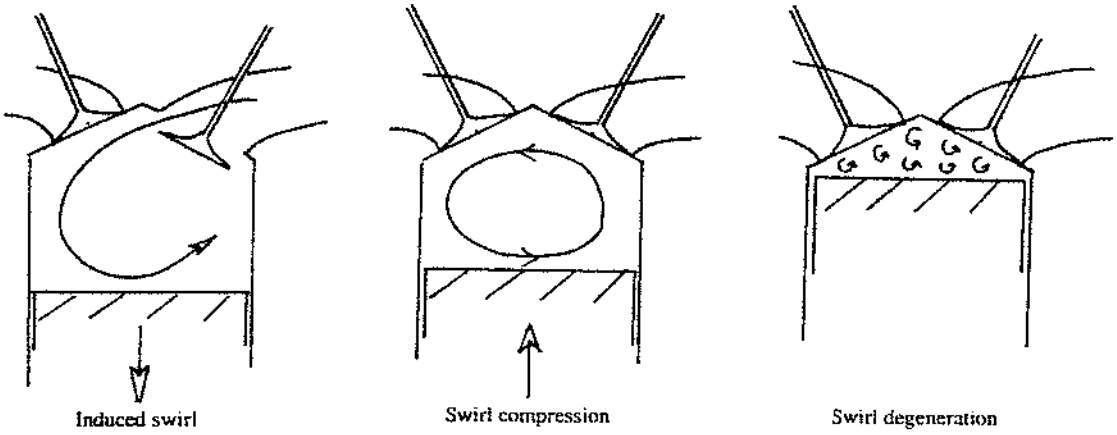

Fig 1 Schematic of barrel swirl behaviour in a four-valve chamber

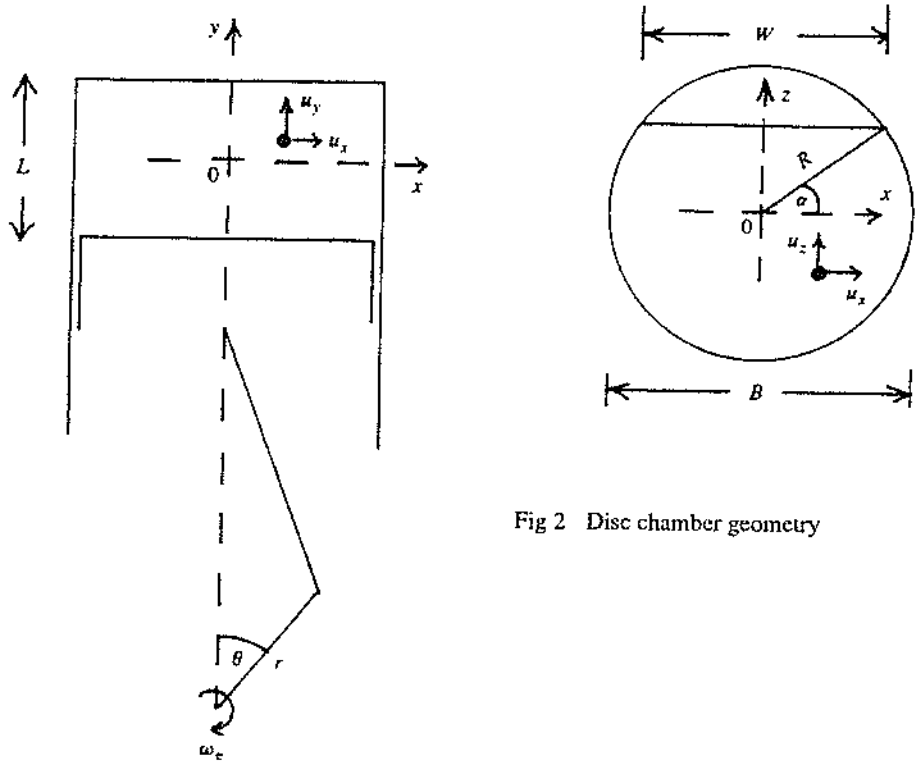

Fig 2 Disc chamber geometry

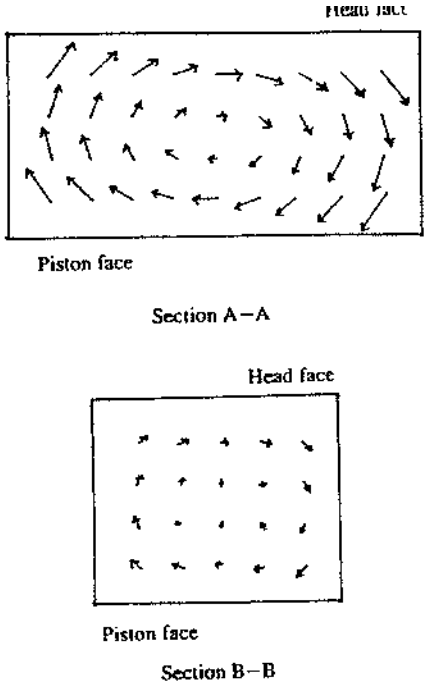

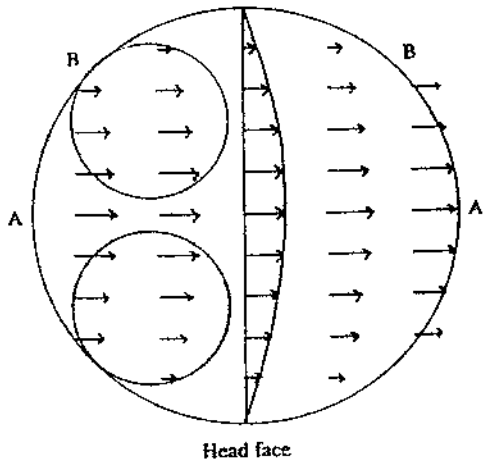

Fig 3 Velocity field across head face and through two vertical sections of the chamber

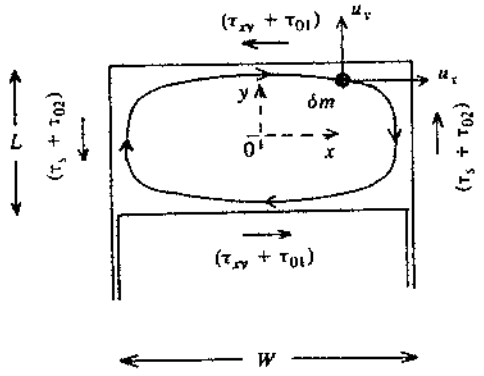

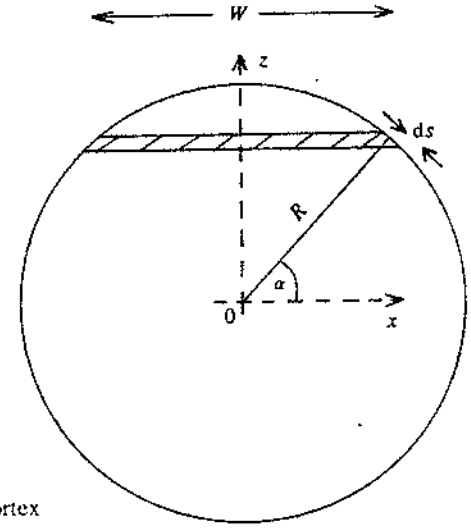

Fig 4 Elemental vortex

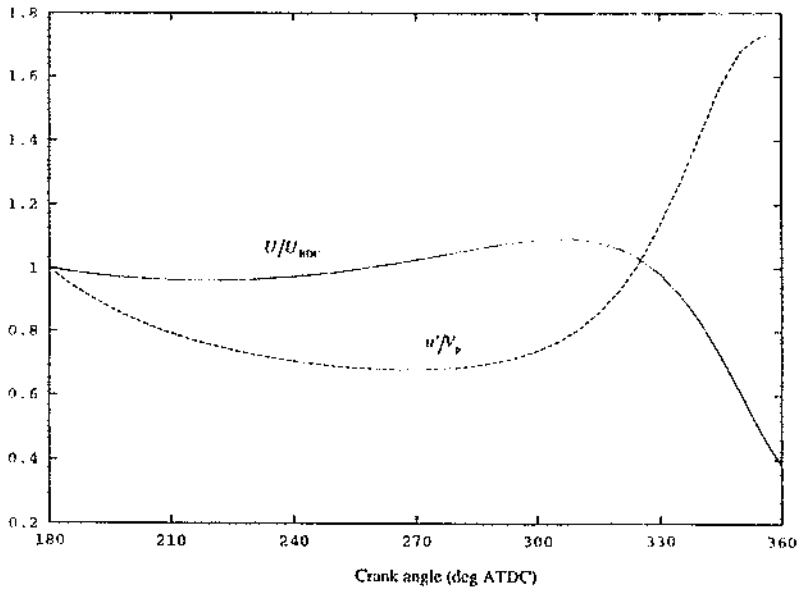

Fig 5 Normalised swirl velocity and turbulence intensity for the reference case

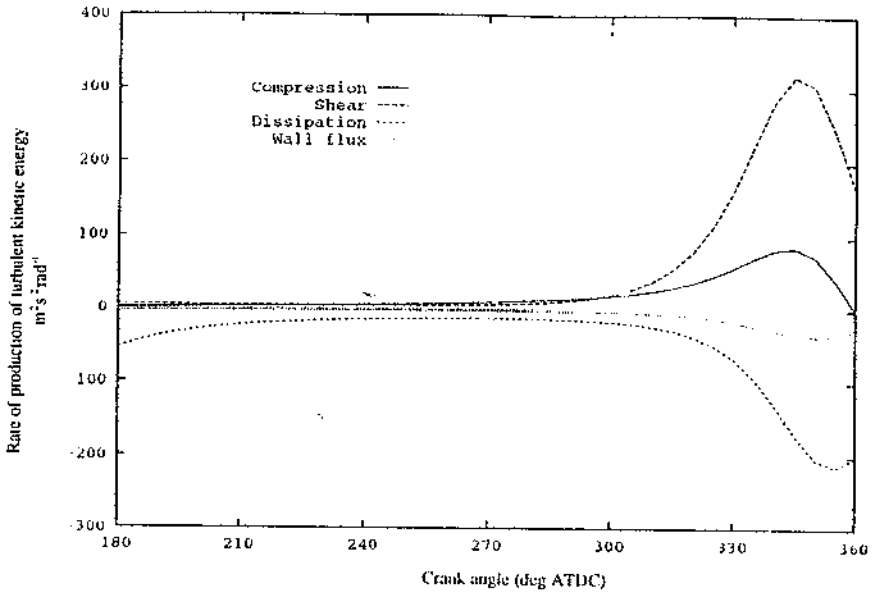

Fig 6 Rate of production of turbulent kinetic energy (k) for the reference case

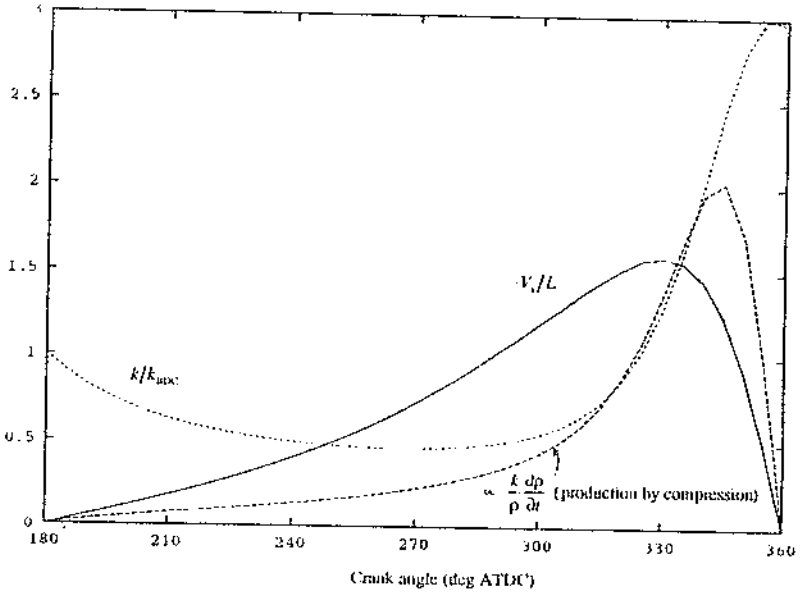

Fig 7 Variation of terms contributing to rate of production of turbulent kinetic energy (k) due to compression for the reference case

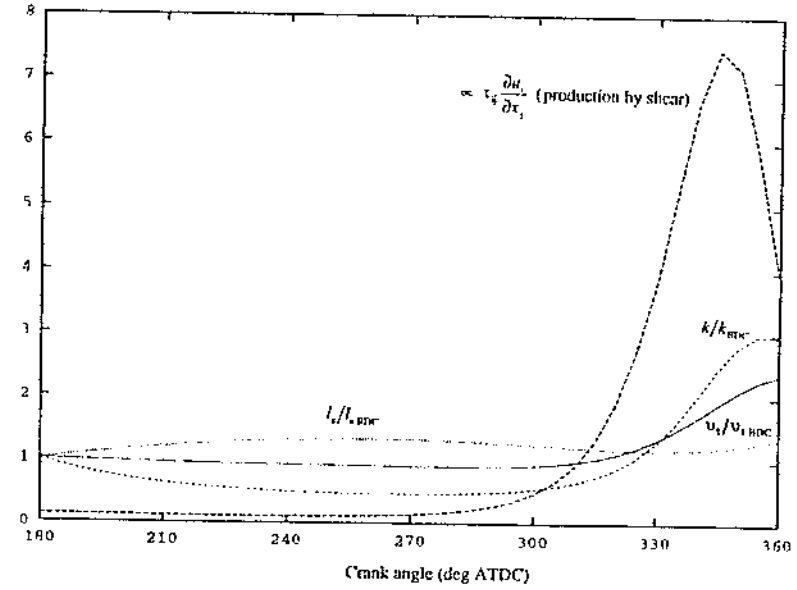

Fig 8 Variation of terms contributing to rate of production of turbulent kinetic energy (k) due to shear for the reference case

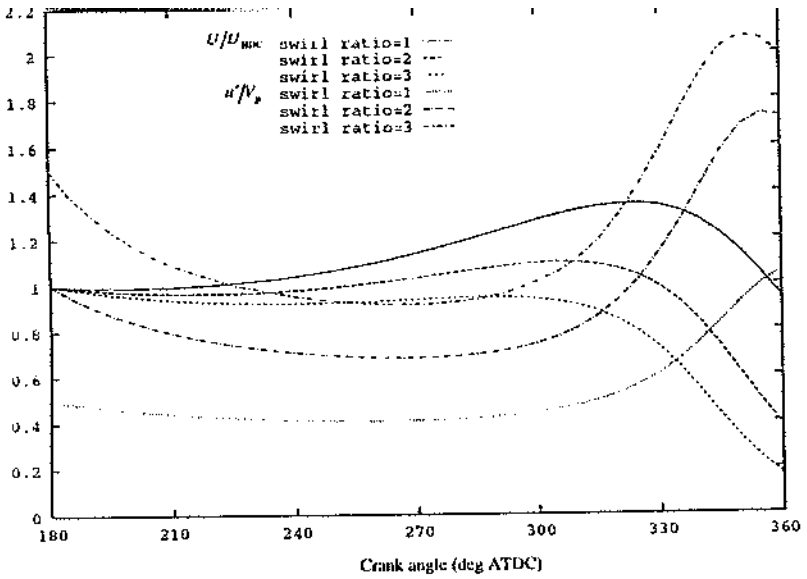

Fig 9 Effect of swirl ratio on normalised swirl velocity and turbulence intensity

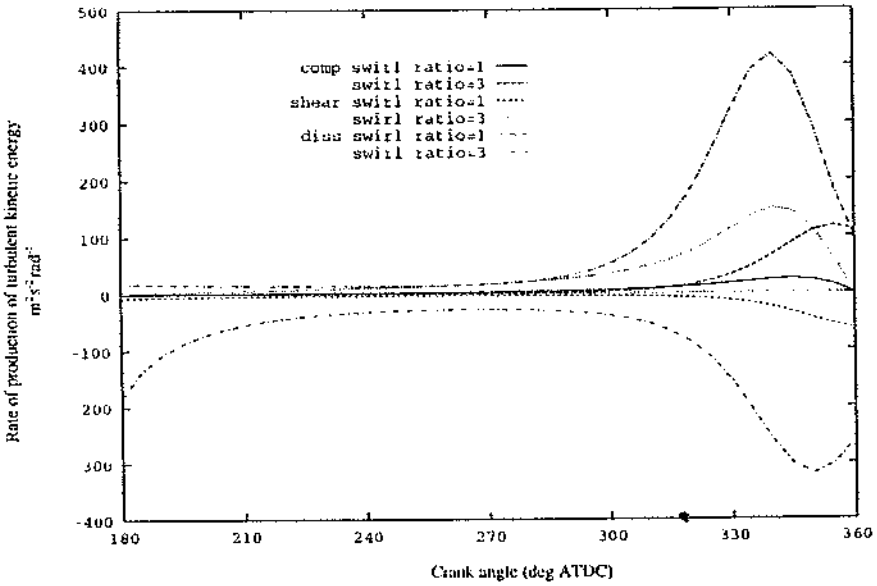

Fig 10 Rate of production of turbulent kinetic energy (k) as a function of swirl ratio

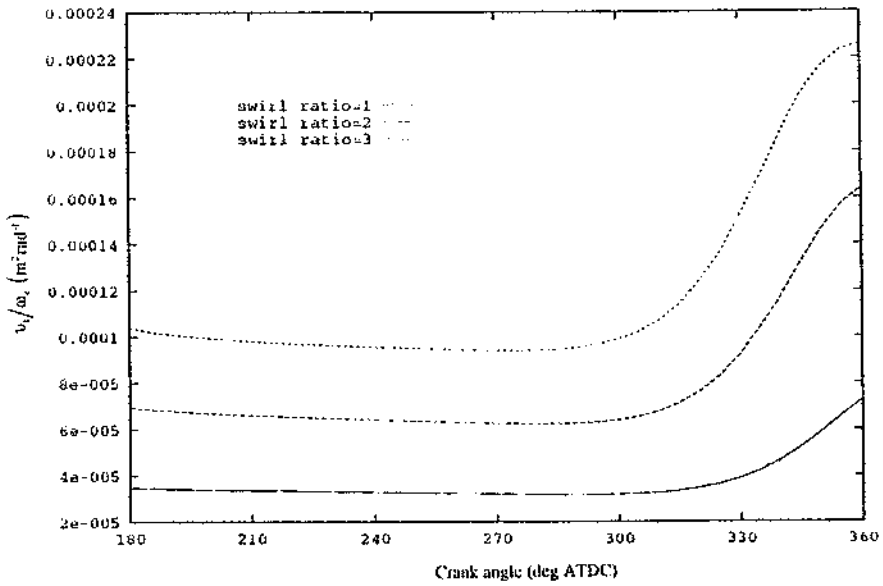

Fig 11 Variation of v_t/ω_e with swirl ratio

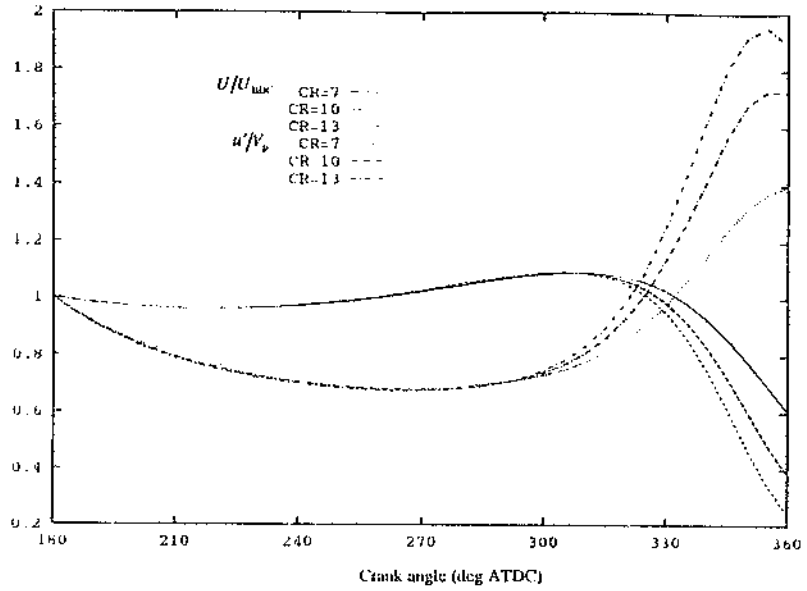

Fig 12 Effect of compression ratio on normalised swirl velocity and turbulence intensity

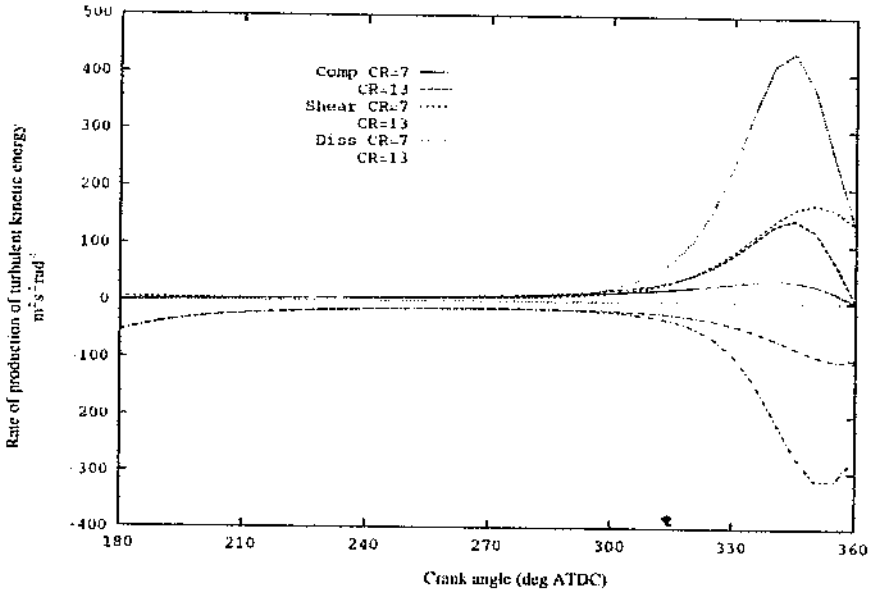

Fig 13 Rate of production of turbulent kinetic energy (k) as a function of compression ratio

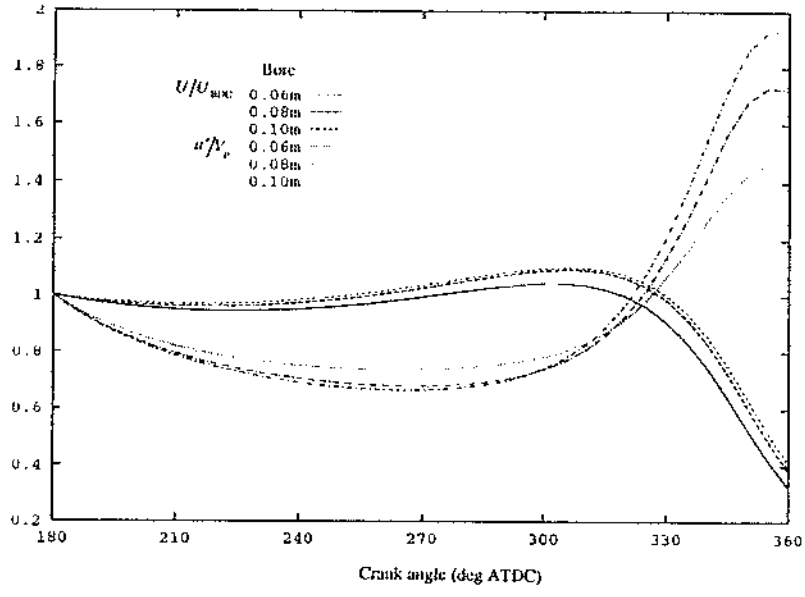

Fig 14 Effect of bore size on normalised swirl velocity and turbulence intensity

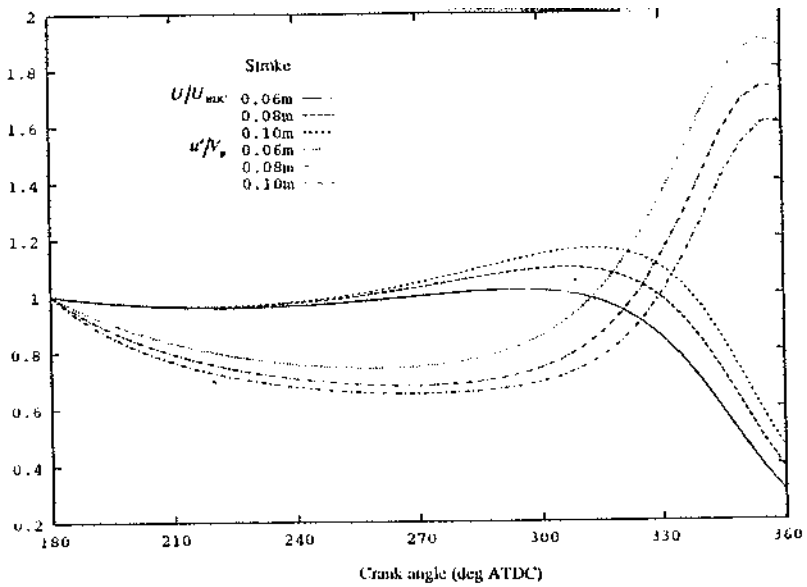

Fig 15 Effect of stroke on normalised swirl velocity and turbulence intensity

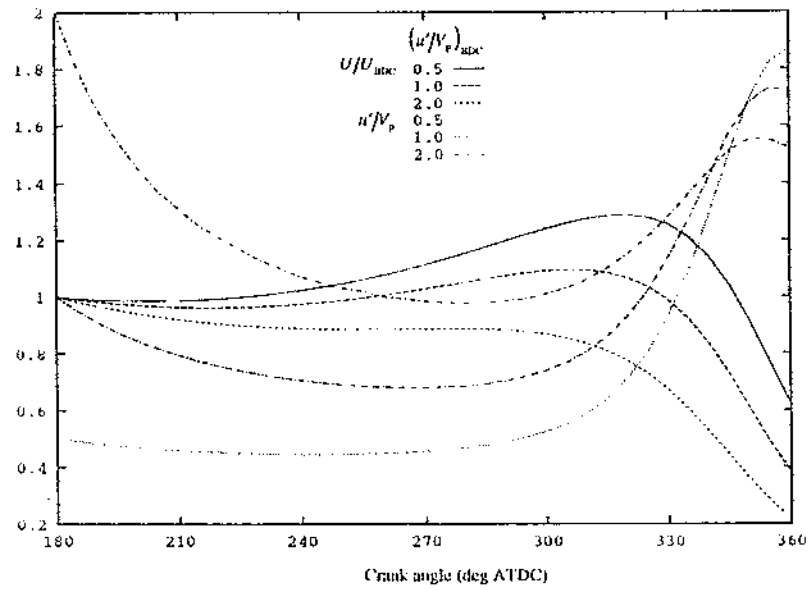

Fig 16 Effect of initial level of turbulence intensity on normalised swirl velocity and turbulence intensity

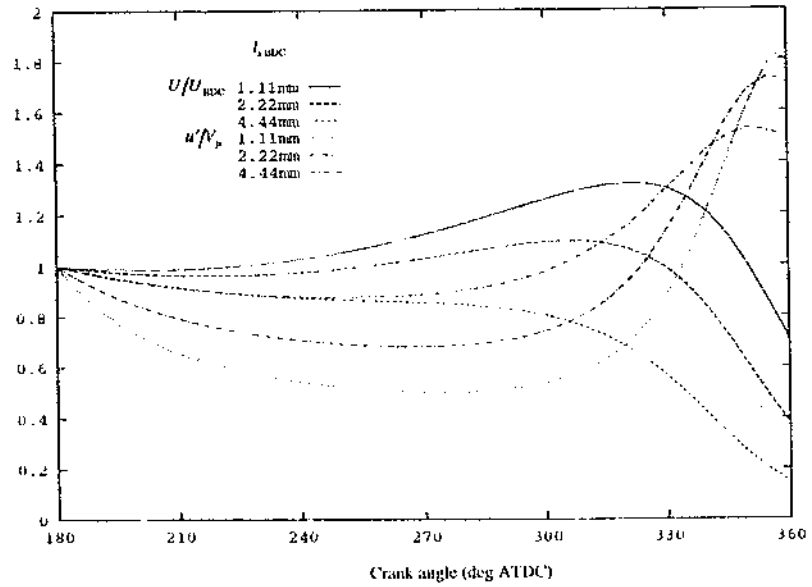

Fig 17 Effect of initial turbulent length scale on normalised swirl velocity and turbulence intensity

APPENDIX

A1 Momentum equation

Consider the elemental vortex as shown in figure 4 and the contribution to the torque from the internal shear stresses τ_s near the cylinder walls acting along an element of thickness ds, height L and width W. Then

$$\tau_s = \left(\tau_{xy}\cos\alpha + \tau_{yz}\sin\alpha\right)$$

The torque T_{s1} resulting from these shear stresses acting on both sides of the vortex is:

$$T_{s1} = \int_{surf} \tau_s WL\ ds = \int_{surf} \left(\tau_{xy}\,dz + \tau_{yz}\,dx\right)WL \qquad (A1)$$

The torque T_{s2} resulting from the stresses τ_{xy} acting near the cylinder head and piston faces is given by

$$T_{s2} = \int_{surf} \tau_{xy} WL\ dz \qquad (A2)$$

Hence the total torque due to the fluid shear stresses acting on the vortex surface is given by

$$T_s = T_{s1} + T_{s2} \qquad (A3)$$

Now $$\tau_{xy} = \rho\upsilon_t\left(\frac{\partial u_y}{\partial x} + \frac{\partial u_x}{\partial y}\right)$$

and $$\tau_{yz} = \rho\upsilon_t\left(\frac{\partial u_z}{\partial y} + \frac{\partial u_y}{\partial z}\right) = \rho\upsilon_t\frac{\partial u_y}{\partial z}$$

Using the flow field prescription given in section 2.1 and noting that $u_x = 0$ on the cylinder walls and $u_y = 0$ on the piston and head faces then, on the walls,

$$\tau_{xy} = -\frac{2U\rho\upsilon_t}{W}\left(1 - \frac{z^2}{R^2}\right) \quad \text{and} \quad \tau_{yz} = \frac{U\rho\upsilon_t z}{R^2} \qquad (A4a)$$

and on the piston and head faces,

$$\tau_{xy} = -\frac{2U\rho\upsilon_t}{L}\left(1 - \frac{z^2}{R^2}\right) \qquad (A4b)$$

Substituting equations (A4a) into (A1) and (A4b) into (A2) and integrating gives (from equation (A3))

$$T_s = \frac{3UM\upsilon_t}{2}\left(\frac{1}{L} + \frac{16}{9\pi B}\right)$$

Consider now the contribution to the torque from the wall friction stresses ,τ_w. It will be assumed that these stresses will be of the same form as that due to the flow over a flat plate, that is

$$\tau_w = \frac{1}{2}\rho V_{wall}^2 C_f$$

where

V_{wall} = velocity at the wall

C_f = friction coefficient

with $C_f = 0.074R_e^{-0.2}$

To estimate the torque due to wall friction consider again an elemental slice of the vortex as shown in figure 4. The surface friction stresses at the piston and head faces are denoted by τ_{01} and those at the cylinder walls by τ_{02}. Hence the torque from the head and piston faces T_{w1} is given as

$$T_{w1} = \int_{surf} \tau_{01} WL\ dz = \frac{1}{2}\rho C_f \int_{surf} u_x^2 WL\ dz \qquad (A5a)$$

and the torque from the walls is T_{w2} given by

$$T_{w2} = \int_{surf} \tau_{02} WL\ ds = \frac{1}{2}\rho C_f \int_{surf} u_y^2 WL\ ds \qquad (A5b)$$

where to a first approximation an average value of C_f has been taken over the surfaces.

Hence

$$T_w = T_{w1} + T_{w2} \qquad (A6)$$

$$u_x = -u_y = \frac{U}{R^2}\left(R^2 - z^2\right) \qquad \text{(A7)}$$

Hence substituting equations (A7) into (A5) and integrating gives from equation (A6)

$$T_w = 0.72 C_f M U^2$$

Hence the total torque, $T = T_s + T_w$ is given by

$$T = \frac{3UM\upsilon_t}{2}\left(\frac{1}{L} + \frac{16}{9\pi B}\right) + 0.72 C_f M U^2$$

It remains to find an expression for the angular momentum of the vortex. Consider a particle of fluid of mass δm (as shown in figure 4). Its angular momentum about 0 is:

$$\left(u_x y - u_y x\right)\delta m$$

Hence the total angular momentum Ω is given by

$$\Omega = \int_{vol}\left(u_x y - u_y x\right)\rho \, dx \, dy \, dz$$

which becomes

$$\Omega = \frac{16U\rho}{R^2}\int_0^{\frac{L}{2}}\int_0^R\int_0^{\sqrt{R^2-z^2}} \frac{y^2\left(R^2 - z^2\right)}{L} + \frac{x^2\sqrt{R^2 - z^2}}{2} \, dx \, dy \, dz$$

Evaluating this integral gives

$$\Omega = \frac{MU}{8}(L + 1.81R) \qquad (3)$$

Finally then as $\frac{d\Omega}{dt} = -T$ we have

$$\frac{d}{dt}\left\{\frac{MU}{8}(L + 1.81R)\right\} = -\frac{3UM\upsilon_t}{2}\left(\frac{1}{L} + \frac{16}{9\pi B}\right)$$

$$-0.72 C_f M U^2 \qquad (4)$$

A2 Turbulence equations

The equations describing the rate of change of k and ε within the combustion chamber volume are as follows:

$$\int_{vol}\rho\frac{dk}{dt} \, dV = \int_{vol}\left(\frac{2}{3}k\frac{d\rho}{dt} + \tau_{ij}\frac{\partial u_i}{\partial x_j} - \rho\varepsilon\right) dV + \int_{surf}\text{Flux}_k \, dS$$

$$\int_{vol}\rho\frac{d\varepsilon}{dt} \, dV = \int_{vol}\left(\frac{4}{3}\varepsilon\frac{d\rho}{dt} + C_{\varepsilon 1}\frac{\varepsilon}{k}\tau_{ij}\frac{\partial u_i}{\partial x_j} - \rho C_{\varepsilon 2}\frac{\varepsilon^2}{k}\right) dV + \int_{surf}\text{Flux}_\varepsilon \, dS$$

and with ρ, k, and ε assumed constant throughout the chamber volume then the integrals can be evaluated as below:

$$\int_{vol}\rho\frac{dk}{dt} \, dV = M\frac{dk}{dt}$$

$$\int_{vol}\frac{2}{3}k\frac{d\rho}{dt} \, dV = M\frac{2k}{3\rho}\frac{d\rho}{dt} = -M\frac{2k}{3L}\frac{dL}{dt}$$

$$\int_{vol}\tau_{ij}\frac{\partial u_i}{\partial x_j} \, dV = \rho\upsilon_t\int_{vol}\left(\frac{\partial u_i}{\partial x_j} + \frac{\partial u_j}{\partial x_i}\right)\frac{\partial u_i}{\partial x_j} \, dV =$$

$$\rho\upsilon_t\int_{vol}\left\{\left(\frac{\partial u_x}{\partial y}\right)^2 + \left(\frac{\partial u_y}{\partial x}\right)^2 + \left(\frac{\partial u_x}{\partial z}\right)^2 + \left(\frac{\partial u_y}{\partial z}\right)^2 + 2\frac{\partial u_x}{\partial y}\frac{\partial u_y}{\partial x}\right\} dV$$

and these integrals can be evaluated as below

$$\int_{vol}\left(\frac{\partial u_x}{\partial y}\right)^2 dV = \frac{32U^2}{L^2R}\int_0^{\frac{L}{2}}\int_0^R\int_0^{\sqrt{R^2-z^2}}\left(R^2 - z^2\right)^2 \, dx \, dy \, dz = \frac{5\pi U^2 R^2}{2L}$$

$$\int_{vol}\left(\frac{\partial u_y}{\partial x}\right)^2 dV = \frac{8U^2}{R^4}\int_0^{\frac{L}{2}}\int_0^R\int_0^{\sqrt{R^2-z^2}}\left(R^2 - z^2\right) dx \, dy \, dz = \frac{3\pi U^2 L}{4}$$

$$\int_{vol}\left(\frac{\partial u_x}{\partial z}\right)^2 dV = \frac{128U^2}{L^2R^4}\int_0^{\frac{L}{2}}\int_0^R\int_0^{\sqrt{R^2-z^2}} y^2 z^2 \, dx \, dy \, dz = \frac{\pi U^2 L}{3}$$

$$\int_{vol}\left(\frac{\partial u_y}{\partial z}\right)^2 dV = \frac{8U^2}{R^4}\int_0^{\frac{L}{2}}\int_0^R\int_0^{\sqrt{R^2-z^2}}\frac{x^2 z^2}{\left(R^2 - z^2\right)} \, dx \, dy \, dz = \frac{\pi U^2 L}{12}$$

$$\int_{vol} 2\frac{\partial u_x}{\partial y}\frac{\partial u_y}{\partial x} = -\frac{56U^2R}{15}$$

Hence

$$\rho\upsilon_t \int_{vol} \tau_{ij}\frac{\partial u_i}{\partial x_j}\,dV = \frac{5MU\upsilon_t}{2}\left(\frac{1}{L^2}+\frac{7}{15R^2}-\frac{256}{75\pi RL}\right)$$

Also we have:

$$\int_{vol} \rho\varepsilon\,dV = \varepsilon M$$

Finally the boundary flux term can be evaluated as follows (see Borgnakke et al (11));

$$\int_{surf} \text{Flux}_k\,dS = -\int_{surf} \rho\upsilon_{teq}\left(\frac{k-k_{eq}}{y_{eq}}\right)dS$$

where k_{eq}, ε_{eq}, and υ_{teq} represent equilibrium values in the region close to the wall. In this region the velocity profile is given by:

$$\frac{u}{u^*} = \frac{1}{0.41}\ln y^+ + 5$$

where the friction velocity $u^* = \left(\frac{\tau_w}{\rho}\right)^{0.5}$ and $y^+ = \frac{y_{eq}u^*}{\upsilon}$

where υ is the kinematic viscosity. Hence we have:

$$y_{eq} = \frac{\upsilon}{u^*}\exp 0.41\left(\frac{u}{u^*}-5\right),\ \varepsilon_{eq} = \frac{u^{*3}}{0.41k},\ \text{and}\ \upsilon_{teq} = \frac{C_D k_{eq}^2}{\varepsilon_{eq}}$$

The boundary fluxes are approximated by:

$$\int_{surf} \text{Flux}_k\,dS = -\rho\upsilon_{teq}\frac{(k-k_{eq})}{y_{eq}}.\ \text{surface area}$$

where the fluxes have been calculated for both the cylinder walls and piston/head faces separately. Similar expressions can be derived for the $\varepsilon-$ equation and so finally we obtain:

$$\frac{dk}{d\theta} = -\frac{2}{3L}\frac{dL}{d\theta}k + \frac{5\upsilon_t}{2\omega_e}\left(\frac{1}{L^2}+\frac{28}{15B^2}-\frac{512}{75\pi BL}\right) - \frac{\varepsilon}{\omega_e} -$$

$$\frac{2}{\omega_e}\left\{\frac{\upsilon_{1teq}(k-k_{1eq})}{0.5By_{1eq}}+\frac{\upsilon_{2teq}(k-k_{2eq})}{Ly_{2eq}}\right\} \qquad (5)$$

$$\frac{d\varepsilon}{d\theta} = -\frac{4}{3L}\frac{dL}{d\theta}\varepsilon + \frac{5\upsilon_t}{2\omega_e}\left(\frac{1}{L^2}+\frac{28}{15B^2}-\frac{512}{75\pi BL}\right)\frac{C_{\varepsilon 1}\varepsilon}{k} - \frac{C_{\varepsilon 2}\varepsilon^2}{\omega_e k} -$$

$$\frac{2}{\omega_e}\left\{\frac{\upsilon_{1teq}(\varepsilon-\varepsilon_{1eq})}{0.5By_{1eq}}+\frac{\upsilon_{2teq}(\varepsilon-\varepsilon_{2eq})}{Ly_{2eq}}\right\} \qquad (6)$$

where k_{1eq}, ε_{1eq}, υ_{1teq} and k_{2eq}, ε_{2eq}, υ_{2teq} are the equilibrium values at the cylinder walls and piston/head faces respectively.

A3 Engine geometry

The following expressions can be derived for the given engine geometry:

Chamber height (L)

$$L = l + r(1-\cos\theta) - l\sqrt{\left(1-\frac{r^2}{l^2}\sin^2\theta\right)} + L_{TDC}$$

Instantaneous piston speed (V_s)

$$V_s = \omega_e r\sin\theta + \frac{\omega_e r^2\sin 2\theta}{\sqrt{(l^2 - r^2\sin^2\theta)}}$$

Mean piston speed (V_p)

$$V_p = \frac{2r\omega_e}{\pi}$$

A4 Initial conditions

Equations (4), (5) and (6) were solved with a Runge-Kutta technique using the NAG software library. Initial conditions for the reference case were specified according to Table I where the following definitions have been used:

turbulence intensity	u'/V_p
swirl ratio	$S = \omega/\omega_e$
initial swirl velocity	$U_{BDC} = r\omega$
initial length scale	$l_s = 0.025L_{BDC}$